AIAA JOURNAL
Vol. 38, No. 9, September 2000

Ionizing Nitrogen and Air Flows in a Superorbital Expansion Tube

Timothy J. McIntyre,* Alexis I. Bishop,† Amberyn M. Thomas‡
University of Queensland, Brisbane, Queensland 4072, Australia
Akihiro Sasoh§
Tohoku University, Sendai 980-8577, Japan
and
Halina Rubinsztein-Dunlop¶
University of Queensland, Brisbane, Queensland 4072, Australia

Vehicles on interplanetary missions enter atmospheres at very high (superorbital) velocities. The kinetic energy of the craft causes dissociation of molecules and ionization of all of the species present in the gas. Ground-based testing of such conditions in nitrogen has been performed in a new superorbital expansion tube, X2, using two optical techniques. Emission measurements identified sources of visible radiation that may influence optical measurements and can also contribute to radiative heat transfer. As well, the emission spectra from Stark-broadened hydrogen lines were used to measure electron concentrations between the bow shock and the body. Two-wavelength holographic interferometry was used to provide two-dimensional density and electron concentration profiles of the flow. Peak electron levels of around $(4.0 \pm 0.6) \times 10^{16}$ cm^{-3} were observed that agreed well with equilibrium estimates. A gradual increase in electron population after the shock was observed, reaching a maximum of about one-quarter of the distance from the body to the shock along the stagnation streamline. Thereafter the concentration decreased because of the influence of the body. Comparisons were also made between flows over different sized cylinders and between air and nitrogen flows.

Nomenclature

G = Gladstone–Dale coefficient
K = a constant
l = path length
N = electron number density
p = fringe shift
r = ratio of Gladstone–Dale coefficient of the ion to that of the atom
λ = wavelength
ρ = density

Subscripts

A = atomic or molecular species
e = electron
N = nitrogen atoms
N_2 = nitrogen molecules
1 = wavelength λ_1
2 = wavelength λ_2
∞ = freestream

Introduction

A VEHICLE reentering the Earth's atmosphere at velocities greater than those of orbiting vehicles has sufficient kinetic energy to cause ionization of the air passing through the bow shock of the body. The presence of electrons behind the bow shock may have a significant effect on the shock stand-off and flow conditions. As well, high levels of radiative heat transfer are expected. Few experiments have been performed at these high velocities and studies are required to aid in the understanding of the flow.

Free-piston-driven shock tunnels have shown their capabilities for simulating orbital reentry, obtaining velocities around 5–8 km/s. A test gas is shock heated and compressed before expanding steadily through a supersonic nozzle. A free-piston driver is utilized to obtain higher enthalpies than that achievable with a cold driver. Related to the work here, experiments have been performed in such a facility providing important details about the dissociation of a nitrogen test gas as it flowed over various diameter cylinders,[1] and ionization of argon.[2] These types of facilities are, however, limited in the speeds they can generate because of radiation losses in the stagnation region at the entrance to the nozzle. To obtain higher freestream velocities, it is necessary to accelerate the gas using an unsteady expansion, eliminating the need to stagnate the flow. Expansion tunnels exploit this method to generate higher velocities, although this is at the expense of reduced test times and flow diameter. Coupling a free-piston driver with an expansion tube allows the simulation of velocities far above Earth orbital reentry velocities, and these facilities are hence termed superorbital.

A series of superorbital expansion tubes have been developed at the University of Queensland beginning with a pilot facility, X1,[3] and culminating in a large-scale tunnel, X3, currently under construction. X1 is capable of generating flows with velocities up to 14 km/s using test gases such as air, nitrogen, and carbon dioxide with test times of the order of 20–100 μs. Our initial experiments in this facility[4] consisted of investigating the flow around a cylinder and a sphere. Emission spectroscopy was used to identify radiating species in the flow and to examine possible influences on the use of other optical techniques. A byproduct of these studies was the observation of Stark-broadened atomic hydrogen lines that allowed the measurement of electron concentrations. This was compared with results obtained using a separate technique, two-wavelength holographic interferometry, which gave two-dimensional electron distributions. Both methods gave values significantly lower than that predicted by a simple equilibrium calculation.

The newer, larger facility, X2, is the focus of the current study. Through the use of a larger diameter core flow, this tunnel allows us to address some of the problems associated with size in X1.

Presented as Paper 98-2772 at the AIAA 20th Advanced Measurement and Ground Testing Technology Conference, Albuquerque, NM, 15–18 June 1998; received 3 March 1999; revision received 7 January 2000; accepted for publication 12 January 2000.

*Senior Research Fellow, Centre for Hypersonics, Department of Physics. Member AIAA.
†Postgraduate Student, Centre for Hypersonics, Department of Physics.
‡Associate Lecturer, Centre for Hypersonics, Department of Physics.
§Associate Professor, Shock Wave Research Centre, Institute of Fluid Science, 2-1-1 Katahira, Aoba. Associate Fellow AIAA.
¶Professor, Centre for Hypersonics, Department of Physics.

Specifically, drawbacks of the earlier experiments included the aspect ratio (length to diameter) of the cylinder, and the complications introduced into the data reduction by the use of an air test gas. Larger models have been manufactured for use in X2 to overcome these problems and tests have been performed with both nitrogen and air test gases. As well, signal levels in the previous experiments were lower than ideal, which introduced unwanted noise in the spectroscopic measurements.

The goal of the experiments presented here was the quantification of the flow around a cylinder for comparison with planned computational fluid dynamics calculations. Emission experiments have been performed to enable comparison of radiating species with those observed in other tunnels, and to study ionization levels. Two-dimensional quantitative density and electron concentration measurements have been performed using our two-wavelength holographic interferometry technique.

Facility

The experiments were performed in the superorbital expansion tube X2, shown in Fig. 1. This free-piston-driven expansion tube has a total length of around 20 m with internal diameter at the tube exit of 85 mm. The driver gas is compressed in a two-stage process using a compound piston launched using a double diaphragm arrangement. Initial compression occurs in a 273-mm-diam tube at comparatively low pressures. Higher pressures are achieved after the heavier central part of the piston detaches and passes into a tube with a diameter of 91 mm terminated by the primary diaphragm. Beyond this, the tube operates as a conventional expansion tube. The test gas is shock heated in the shock tube and then expanded unsteadily to the test condition through the accelerator tube. Comparisons are made with similar experiments conducted in the smaller X1 facility, which has a secondary driver between the main driver and the shock tube. This section allows for an increase in the temperature of the driver gas that generates stronger primary shock waves in the test gas. As the current configuration of X2 does not include such a section, similar freestream velocities to X1 are generated only at lower densities.

Instrumentation on the tunnels include pressure transducers at regular intervals along the shock and expansion tubes. The latter are used to infer the freestream flow velocity by assuming that the Mirels condition is satisfied whereby the test slug maintains a constant length because gains from gas processed by the shock wave are matched by losses through the boundary layer. The freestream velocity is thus equal to the measured shock velocity. This has been experimentally confirmed at similar conditions in X1 using laser-enhanced ionization flow tagging to measure the free-stream velocity directly.[5]

Calculated test gas conditions in X2 together with conditions used in X1[4] are given in Table 1. The calculations used for the X1 facility were based on the TUBE program.[3] This program uses the shock tube fill pressure and shock velocity together with the expansion tube shock velocity to determine the freestream conditions. The simulation is one dimensional, ignores viscous effects, and assumes chemical equilibrium. Calculated freestream static pressures were within experimental uncertainty of the measured static pressure. Similar calculations for the X2 facility severely overpredicted the measured static and pitot pressure. A revised calculation,[6] based on a two-dimensional shock-capturing code,[7] was performed that more accurately modeled the measured parameters (velocities and pressures). This analysis started at the secondary diaphragm and computed the transient flow in the accelerator tube. Conditions behind the incident shock in the shock tube together with the fill pressure in the expansion tube were used to calculate freestream conditions. Chemical equilibrium was again assumed and viscous effects were accounted for using laminar boundary layers. Studies are ongoing to determine the importance of these assumptions.

The current investigation was restricted to studying two-dimensional flows over cylinders. This type of model is preferable for the interferometry measurements as it allows for easier data analysis. A small cylinder with a diameter of 15 mm and a length of 60 mm was used in both the interferometry and the emission spectroscopy. A larger model with a diameter of 30 mm and a length of 60 mm was also studied using interferometry, although the flow here can no longer be considered two dimensional.

Experimental Arrangement

Emission

The main aim of the emission studies was to provide an independent measurement of the electron concentration using Stark broadening of hydrogen lines. This process is well understood, with the line widths of the H-α, H-β, and H-γ lines being directly related to the electron concentration with only minor influences from other flow parameters such as temperature at the flow conditions investigated here. The emission studies were also used to identify radiating species in the flow. This type of investigation often provides qualitative data on impurities in the flow. Previous studies have established the presence of a variety of contaminants in X1.[4] At moderate velocities (around 4–5 km/s), the spectral distribution of the emission was similar to the results of measurements in other high enthalpy facilities.[8,9] For superorbital conditions (11 km/s), the spectra showed a continuous background signal and far fewer spectral lines. Here, we report the results of a similar study for flows produced in X2.

The experimental arrangement used was identical to that reported in our previous study.[4] The region along the stagnation streamline in front of the cylinder was imaged through an imaging spectrometer (SPEX 270M) onto a fast-gated intensified charge-coupled device (CCD) camera (Princeton Instruments) that has an ultraviolet-enhanced photocathode. This arrangement yields a spectrally resolved image along one spatial direction. Each image covered a region of approximately 70 nm, with spectra recorded in

Table 1 Calculated conditions in the freestream and behind a bow shock in the X2 and X1 superorbital expansion tubes (assuming chemical and thermal equilibrium)

	A. X2 (N_2)		B. X1 (Air)	
Condition: parameter	Freestream	Bow shock	Freestream	Bow shock
Pressure (kPa)	1.3	140	29	850
Temperature (K)	3,030	10,700	7,160	15,900
Density (kg/m^3)	0.0014	0.021	0.0079	0.072
Enthalpy (MJ/kg)	64	64	93	93
Velocity (km/s)	10.3	0.7	10.8	1.2
Mach number	9.6	0.2	4.7	0.29
Dissociation fraction N_2	0.0	1.0	0.78	1.0
Dissociation fraction O_2	——	——	1.0	1.0
Ionization fraction N	——	0.04	——	0.31
Ionization fraction O	——	——	——	0.21
Electron concentration (cm^{-3})	——	3.6×10^{16}	——	8.8×10^{17}

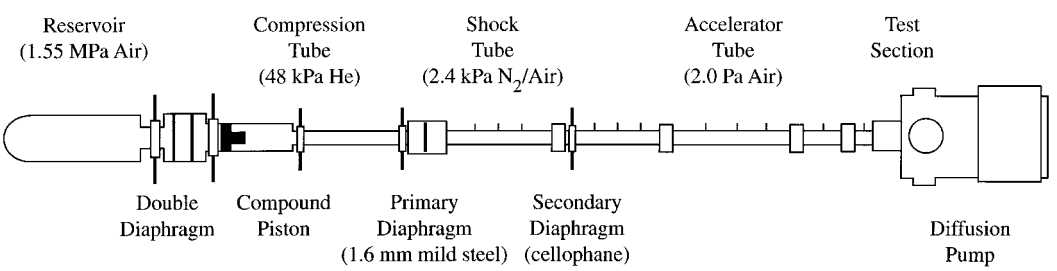

Fig. 1 Schematic diagram of the superorbital expansion tube X2.

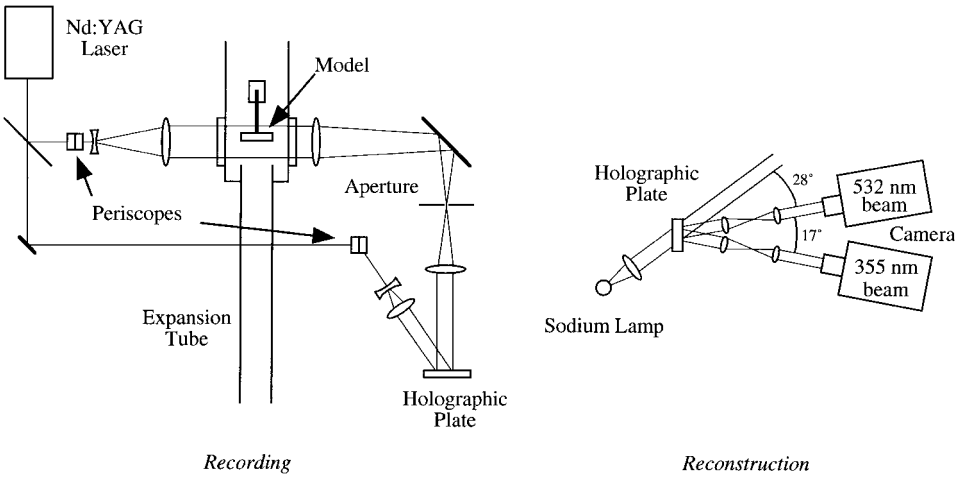

Fig. 2 Experimental arrangement for holographic interferometry.

successive shots covering wavelengths in the 200–700 nm range. Intensity and resolution of the images were controlled by a combination of spectrometer entrance slit size (50 μm) and the length of the camera gate (1 μs). With these settings, the spectral resolution of the spectrometer was estimated to be 0.3 nm.

Holographic Interferometry

We have previously reported the development of a two-wavelength holographic interferometry technique that we have used to measure electron concentrations in high enthalpy flows.[10] Here, the technique was implemented in X2 with the layout for measurements shown in Fig. 2. The 1064 nm output of a pulsed, seeded Nd:YAG laser was frequency doubled to provide light at 532 nm. Part of this light, combined with the fundamental infrared beam, was used to simultaneously generate light at 355 nm. The two wavelengths were combined and passed collinearly through the holographic interferometry system. This consisted of the test arm that contained the test section, and the recording arm that passed the beams around the tunnel. Light from the two arms was overlapped on a holographic plate forming holograms of the test section. In total, four holograms were recorded on a plate during a measurement—one at each wavelength prior to the flow, and one at each wavelength (simultaneously) during the flow. Afterward, the plate was developed and the images reconstructed using a sodium lamp. Interferograms were formed where the "no-flow" and "with-flow" images overlap. The interferogram resulting from the recording with the 532-nm beam is spatially separated from that recorded with the 355-nm beam. The interferograms were recorded on a 1524 × 1012 pixel Kodak DCS410 CCD camera and transferred to a computer for analysis.

At the conditions used in this study, the freestream consisted almost entirely of molecular nitrogen, which is dissociated across the shock leaving a flow of atomic nitrogen. This is then ionized within the relaxation zone between the shock and the body. The presence of the molecular nitrogen complicates the data reduction as molecular and atomic nitrogen have different Gladstone–Dale coefficients and hence contribute to the gas refractivity (and hence fringe shift) by different amounts for the same density. It is assumed that the less energetic dissociation process occurs rapidly behind the bow shock, so that the observed fringe shift across the shock is because of the increase in density of the gas as well as the change in refractivity because of the change in composition. This assumption can have a major effect on the measured total density of the technique, but has a much smaller influence on the determined electron concentration.

The total density ρ and the electron concentration N_e can be determined using the equations[10]

$$\rho = \rho_\infty + \frac{\left(p_1 - p^*_{1\infty}\right)\lambda_1 K_2 - \left(p_2 - p^*_{2\infty}\right)\lambda_2 K_1}{(G_1 K_2 - G_2 K_1)l}$$

$$N_e = N_{e\infty} + \frac{\left(p_1 - p^*_{1\infty}\right)\lambda_1 G_2 - \left(p_2 - p^*_{2\infty}\right)\lambda_2 G_1}{(G_1 K_2 - G_2 K_1)l}$$

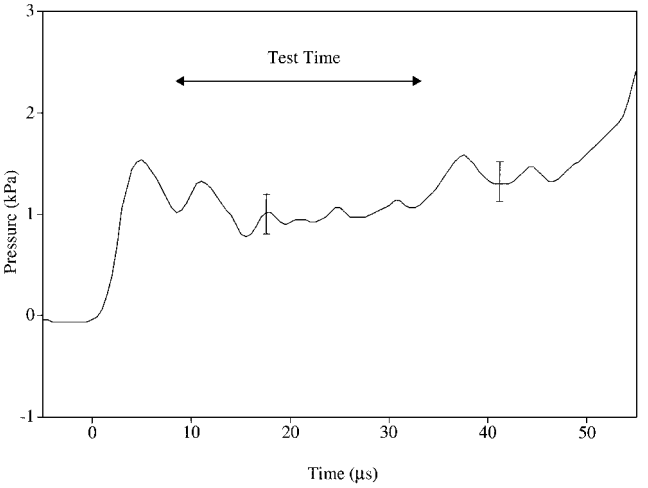

Fig. 3 Static pressure in the freestream of X2 for a nitrogen test gas.

The values of p^*_∞ refer to the freestream fringe shift corrected to allow for the complete dissociation of nitrogen. This is given by

$$p^*_{i\infty} = p_\infty + \left(G_{iN} - G_{iN_2}\right)(6\rho_\infty l/\lambda_i)$$

where subscripts i represent values at the wavelength λ_i. For a flow species A, the constant K_i can be written

$$K_i = K\lambda_i^2 + G_{Ai} m_A (1 - r_A)$$

where m_A is the mass of an atom, and r_A is the ratio of the Gladstone–Dale coefficient for the atom to that for the ion. For the measurements presented here, this is approximated as $r_A = 1$ because of the lack of an experimental measurement of the Gladstone–Dale coefficient for ions. The uncertainty of this value also has only a small influence on the uncertainty in the electron concentration measurement.

Results

Tunnel Performance

Data were recorded over a series of about 30 tests. Pressure transducers were used along the tube to measure shock speeds. Primary shock speeds (in the shock tube) were measured to be 5.0 km/s with a shot-to-shot variation of less than ±5%. Secondary shock speeds (in the accelerator tube) were measured to be 10.3 km/s, also with a variation of less than ±5%. Operating characteristics of the freestream were monitored by recording static and pitot pressures throughout the test time. A sample static pressure trace is given in Fig. 3 showing an approximately constant plateau of around 20–30 μs constituting the test time. The pressure thereafter increases because of the arrival of the unsteady expansion. The biggest uncertainty in these measurements lies in variations during the test time

and shot-to-shot variations rather than the accuracy of the transducers. Based on measurements during the course of the experimental program, the static pressure is estimated to be (1.0 ± 0.2) kPa, which is in reasonable agreement with the calculated value presented in Table 1. The pitot pressure was measured to be (170 ± 30) kPa.

Emission

Emission images were recorded with spatial resolution along the stagnation streamline of the flow. To identify spectral features, the region between the shock and the body was averaged over the spatial direction yielding spectra. The results for the complete wavelength range are shown in Fig. 4, whereas the spectrum over a narrower range, 350–450 nm, is shown in Fig. 5. In each figure, spectra from our previous measurements in X1 are also given (see Table 1 for calculated conditions).[4] Prominent lines over the narrower wavelength range that have been identified are labeled in Fig. 5. The spectra for the current measurements are in general similar to those seen previously. The majority of the radiation lies in the wavelength range 250–450 nm. The most prominent lines are again the two Ca^+ lines just below 400 nm. However, there are a number of notable differences. Firstly, the strong silicon lines at 251 and 390 nm observed in X1 are absent from the X2 spectra. The atomic hydrogen lines (656, 486, and 434 nm) are also significantly weaker. These could possibly be explained by having a better evacuation cycle leading to less contamination. Note that transitions in nitrogen and oxygen atoms are considerably weaker than those for the contaminant metallic species and are thus not observed in the spectra despite the metallic species being present only in trace amounts. Similar results have been obtained in other impulse facilities.[8,9]

The conditions in Table 1 show that the level of ionization in the current experiments is expected to be significantly lower than those in X1. This is experimentally verified as the X2 spectral lines of hydrogen are generally narrower than those measured in X1 despite similar resolution in the detection apparatus. Furthermore, the level of continuum background compared with the strength of the spectral lines is lower in X2. These observations are consistent with a lower electron concentration.

There exist a number of broad structures (355, 385, and 415 nm) that could possibly indicate the presence of molecular species, although at the high temperatures calculated, one would expect that all

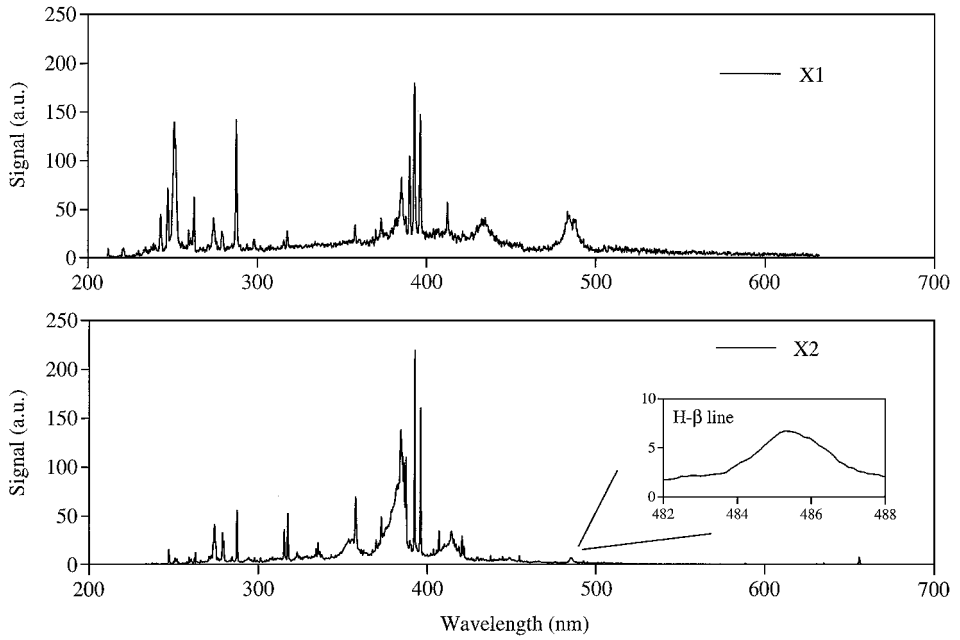

Fig. 4 Emission spectra from the current experiments compared with previous measurements in X1.

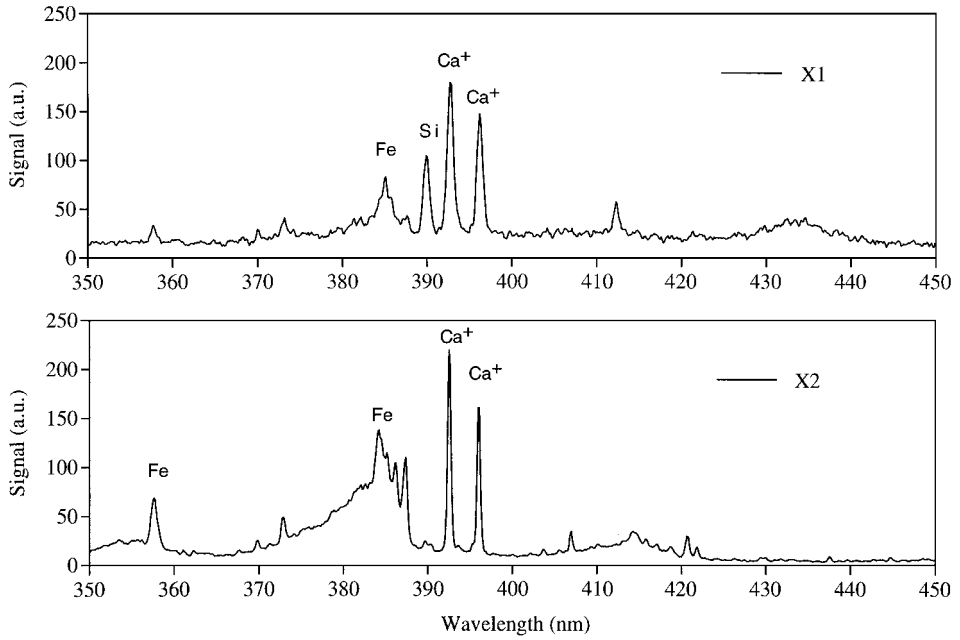

Fig. 5 Emission spectra for a narrower wavelength range from the current experiments compared with previous measurements in X1.

molecules would be dissociated. An alternative explanation is that they are a collection of broadened atomic lines. Further investigation is required to establish their source.

As noted, the atomic hydrogen lines can be used to determine electron concentrations through an analysis of Stark broadening. The lines H-α (656.3 nm) and H-β (486.1 nm) were identified in the spectra but were considerably weaker than previously observed. Nevertheless, signal levels were sufficient to make a reliable measurement of the linewidths. The H-γ (434.1 nm) was too weak to be detected.

The line shape of the H-β line was used to determine the electron concentration. To achieve this, the region between the shock and the body of the images was divided into strips 10 pixels wide. Each of these strips was individually averaged, yielding line shapes at various locations along the stagnation streamline. The resulting profiles were compared with numerical simulations[11] that used a well-developed model to predict line shapes as a function of electron concentration. The model line shapes included components because of Doppler and Stark broadening and were corrected for the 0.3-nm resolution of the spectrometer. In general, Stark broadening gave linewidths of the order of 1–2 nm, several orders of magnitude larger than the Doppler broadening expected at the conditions behind the bow shock. The results for all of the regions were plotted as a function of position yielding an electron distribution between the shock and the body as shown in Fig. 6. The electron concentration is seen to rise to a peak value of about $(3.5 \pm 1.0) \times 10^{16}$ cm^{-3}, some three-quarters of the way from the shock to the body. Because of the low concentration of hydrogen in the tunnel, the signal levels were low. Furthermore, the lower electron concentrations for the measurements in X2 have led to results with larger uncertainties compared with those in X1.

Holographic Interferometry

Interferograms were recorded of nitrogen and air flows over a 15-mm-diam cylinder and of nitrogen flows over a 30-mm-diam cylinder. The results are presented separately next.

The focus of the current study was the flow of nitrogen at a velocity of around 10 km/s over a cylinder. The diameter of the cylinder was

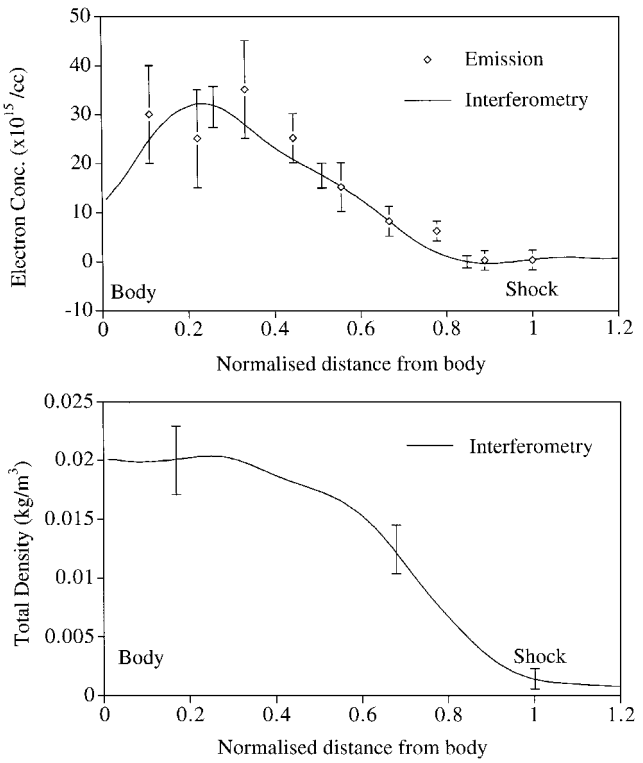

Fig. 6 Measured electron concentrations along the stagnation streamline for nitrogen flow over the small cylinder. Uncertainties for the emission studies are shown at each measurement point, although only typical values for the interferometry results are given.

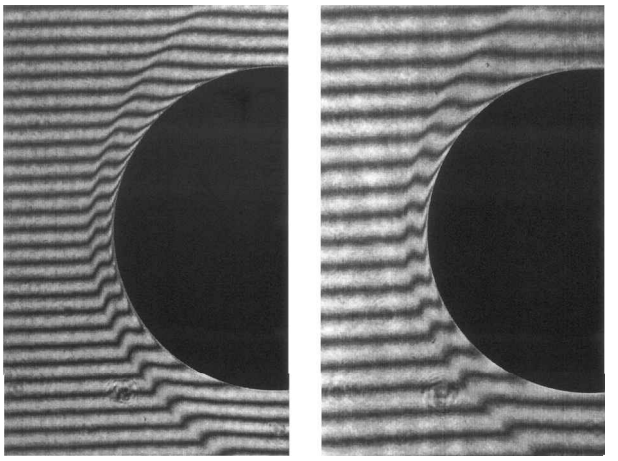

Fig. 7 Raw holographic interferograms of nitrogen flowing over a 15-mm-diam cylinder. Flow is from left to right. Left image: recorded with a wavelength of 355 nm; right image: recorded with a wavelength of 532 nm.

set by the desire to have an aspect ratio (length to width) greater than three to minimize edge effects. A cylinder with a length of 60 mm was thus chosen with a diameter of 15 mm. Sample images of the flow of nitrogen over the cylinder at the conditions given in Table 1 are shown in Fig. 7. These are simultaneously recorded interferograms of the flow at two separate wavelengths. The image recorded at 355 nm has a greater sensitivity to the presence of heavy particles (atoms, ions, molecules), whereas the 532-nm image has a greater sensitivity to electrons.

Away from the center of the body, the fringes show a small shift across the oblique shock. This can be interpreted as the direction for a positive shift, as the strength of the shock is too weak at this point to generate any electrons that would cause a negative fringe shift. Along the stagnation streamline, both images show an initial positive fringe shift because of the increase in density across the shock. Also contributing to this shift is the dissociation of molecular nitrogen. Using the conditions given in Table 1, an estimate of the shifts expected from each component can be made. The shift because of density increase at 355 nm is calculated to be 0.4, whereas that because of the dissociation of nitrogen is of the order of 0.15. Behind the shock front, the 532-nm image shows a reversal in fringe direction indicative of the liberation of electrons. The 355-nm image does not show this shift indicating that the effect is indeed because of the presence of electrons.

The images were processed using a Fourier transform technique together with phase unwrapping,[10] to yield a two-dimensional phase distribution for each wavelength. The fringe spacings in the interferograms were chosen so that the peaks in the Fourier transform plane corresponding to the fringe frequency were well separated from the zero-order peak, allowing effective filtering. The carrier fringes for the two wavelengths are not independent—the spacings for the interferogram recorded at 532 nm are about one and a half times those for the 355-nm interferogram. Finer fringes can lead to problems with the unwrapping algorithm because of the scale of the noise and imperfections in the optics as present in the images. The phase distributions at each wavelength were combined using the equations given in the Experimental Arrangement section to obtain simultaneous measurements of electron concentration and density; these are shown in Fig. 8. In calculating these values, it was assumed that the freestream electron concentration was zero, and that the freestream density was the calculated value presented in Table 1. Uncertainties are based on the accuracy of the phase retrieval method together with uncertainties because of the assumptions discussed in the Experimental Arrangement section. A full analysis can be found elsewhere.[10] As the freestream density is very low, uncertainties in using the calculated value have only a small effect on the values determined between the shock and the body, far below that because of other uncertainties. The results show that electrons are liberated in only a small region in the vicinity of the front of the cylinder. Values along the stagnation streamline have been extracted and are shown

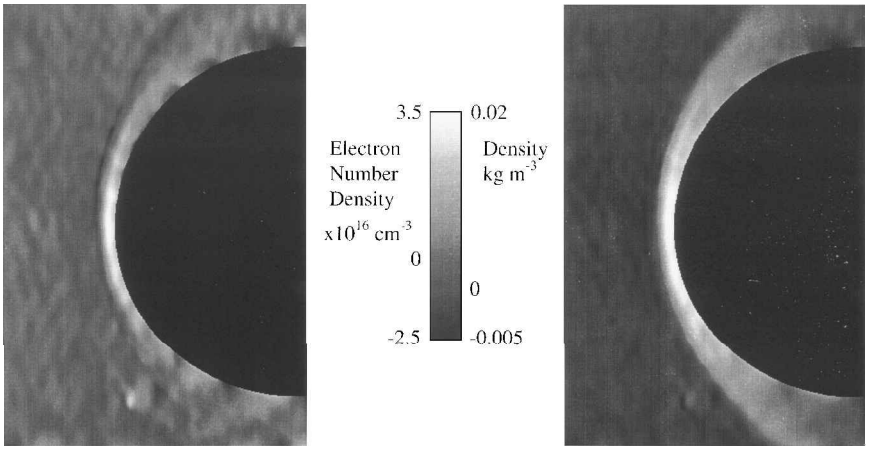

Fig. 8 Measured electron concentration and total density for nitrogen flow over the small cylinder.

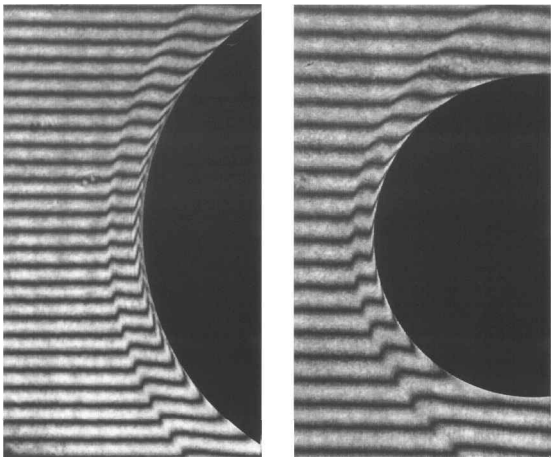

Fig. 9 Raw holographic interferograms recorded with a wavelength of 532 nm. Flow is from left to right. Left image: nitrogen test gas, 30-mm-diam cylinder; right image: air test gas, 15-mm-diam cylinder.

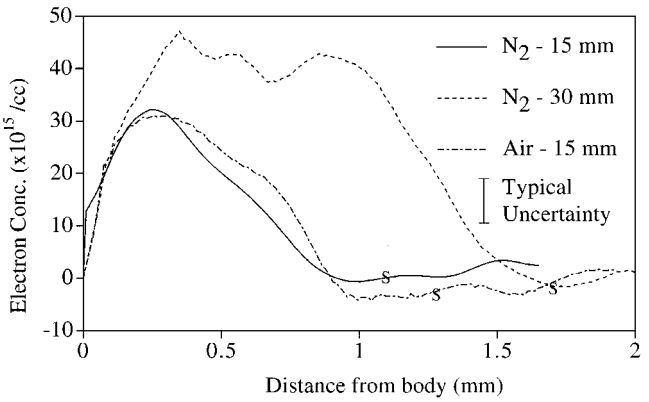

Fig. 10 Measured electron concentrations along the stagnation streamline. S indicates the location of the shock in each case. A typical uncertainty for all curves is shown.

together with the emission results in Fig. 6. For the total density, a plateau value of (0.020 ± 0.003) kg/m^3 is attained in agreement with the calculated equilibrium value given in Table 1. The electron concentration compares favorably with the emission results. The onset of ionization is not immediate behind the shock. At about one-quarter of the distance from the shock to the body, the concentration increases, reaching a maximum of around $(3.0 \pm 0.5) \times 10^{16}$ cm^{-3}, falling below the calculated freestream value. Thereafter it decreases rapidly because of the influence of the body: this effect extends farther into the flow than thermal boundary layers because of the high mobility of the electrons.

A larger-diameter cylinder was studied to generate a bigger distance between the bow shock and the body. Figure 9 shows a holographic interferogram, recorded with a wavelength of 532 nm, of the flow of nitrogen over a 30-mm-diam cylinder. (The corresponding 355-nm image is not shown.) For this case, a larger shock standoff distance is observed compared to that shown in Fig. 7. A small positive fringe shift is observed across the shock followed by a small decrease and then a plateau region. These interferograms were analyzed as before and the electron number density plotted along the stagnation streamline. The result is shown in Fig. 10 together with the earlier case (15-mm-diam cylinder, nitrogen test gas). The figure shows that, for the larger cylinder, there is sufficient time along the stagnation streamline for the flow to reach equilibrium conditions, where the electron concentration reaches a plateau. As this is at a higher concentration than for the small cylinder, it is evident that equilibrium has not been reached for the small cylinder. The measured equilibrium value of $(4.0 \pm 0.6) \times 10^{16}$ cm^{-3} is in agreement with the calculated value presented in Table 1.

Measurements were also performed using air as a test gas instead of nitrogen. An interferogram of an air flow over the 15-mm-diam cylinder is shown in Fig. 9. The freestream velocity and static pressure were measured to be the same here as for nitrogen. However, the pitot pressure was lower at (125 ± 30) kPa. The interferogram shows similar features to that for the nitrogen flow. The electron concentration along the stagnation streamline is shown in Fig. 10. The analysis of these images includes a correction for the presence of oxygen and assumes that the ionization rate of oxygen is equal to that for nitrogen. The influence of these assumptions has a relatively minor effect.[10] There is, in general, good agreement between the air and the nitrogen case, indicating that the electron distribution is relatively insensitive to the presence of the oxygen.

Conclusions

The flow of nitrogen and air over a cylinder has been investigated under superorbital conditions. Emission measurements identified a range of radiating species in the flow including calcium and iron. Observations of the Stark broadening of atomic hydrogen lines allowed an estimation of the electron concentration between the shock and the body. This was more accurately measured with the use of two-wavelength holographic interferometry. Along the stagnation streamline, the onset of ionization was delayed slightly before reaching a maximum about one-quarter of the way out from the body. Thereafter it decreased rapidly because of the presence of the body. Comparisons were made between flow over two different sized cylinders. The rate of ionization and recombination was found to be about the same for both. However, because of the larger shock standoff distance for the larger cylinder, a plateau region of almost constant electron concentration was observed, indicating equilibrium. This showed that equilibrium had not been attained for the small cylinder case. Comparisons were also made between air and nitrogen flows with little difference being observed.

The results show the usefulness of investigating high-velocity flows in superorbital facilities, particularly with emphasis on

ionization processes. Computer simulations are currently in progress for comparison with the results.

Acknowledgments

This work was funded by the University of Queensland and was conducted under an international collaboration project partly funded by the Australian Research Council. The authors would like to thank Robert Palmer and Richard Morgan for their assistance with the experiments. The input from the mechanical and electrical workshops at the Departments of Physics and Mechanical Engineering is gratefully acknowledged.

References

[1]Hornung, H. G., "Non-Equilibrium Nitrogen Flow over Spheres and Circular Cylinders," *Journal of Fluid Mechanics*, Vol. 53, No. 1, 1972, pp. 149–176.

[2]Hornung, H. G., and Sandeman, R. J., "Interferometric Measurements of Radiating Ionizing Argon Flow over Blunt Bodies," *Journal of Physics D: Applied Physics*, Vol. 7, 1974, pp. 920–934.

[3]Neely, A. J., and Morgan, R. G., "The Superorbital Expansion Tube Concept, Experiment and Analysis," *Aeronautical Journal*, Vol. 98, No. 973, 1994, pp. 97–105.

[4]McIntyre, T. J., Bishop, A. I., Thomas, A. M., Wegener, M. J., and Rubinsztein-Dunlop, H., "Emission and Holographic Interferometry Measurements in a Superorbital Expansion Tube," *AIAA Journal*, Vol. 36, No. 5, 1998, pp. 1049–1054.

[5]Littleton, B. N., Bishop, A. I., McIntyre, T. J., Barker, P. F., and Rubinsztein-Dunlop, H., "Flow Tagging Velocimetry in a Superorbital Expansion Tube," *Proceedings of the 21st International Symposium on Shock Waves*, edited by A. F. P. Houwing, Panther Publishing and Printing, Canberra, Australia, 1997, pp. 551–515.

[6]McIntyre, T. J., Jacobs, P. A., Bishop, A. I., and Rubinsztein-Dunlop, H., "Experimental and Numerical Studies of Super-Orbital Ionising Flows," *Proceedings of the 22nd International Symposium on Shock Waves*, Imperial College, London, 1999.

[7]Jacobs, P. A., "MB_CNS: A Computer Program for the Simulation of Transient Compressible Flows; 1998 Update," Dept. of Mechanical Engineering Rept. 7/98, Univ. of Queensland, Brisbane, Australia. URL: http://www.mech.uq.edu.au/staff/jacobs/cfd.

[8]Palma, P. C., Houwing, A. F. P., and Sandeman, R. J., "Absolute Intensity Measurements of Impurity Emissions in a Shock Tunnel and Their Consequences for Laser-Induced Fluorescence Measurements," *Shock Waves*, Vol. 3, No. 1, 1993, pp. 49–53.

[9]Beck, W. H., Müller, M., and Wollenhaupt, M., "Application of Spectroscopic Diagnostic Techniques to Studies on HEG: Preparatory LIF Work and Emission Spectroscopy Results," *15th International Congress on Instrumentation in Aerospace Simulation Facilities*, Franco-German Research Inst. of Saint-Louis, Saint-Louis, France, 1993.

[10]McIntyre, T. J., Wegener, M. J., Bishop A. I., and Rubinsztein-Dunlop, H., "Simultaneous Two-Wavelength Holographic Interferometry in a Superorbital Expansion Tube Facility," *Applied Optics*, Vol. 36, No. 31, 1997, pp. 8128–8134.

[11]Lemke, M., "Extended VCS Stark Broadening Tables for Hydrogen—Lyman to Brackett Series," *Astronomy and Astrophysics Supplement Series*, Vol. 122, April 1997, pp. 285–292.

R. P. Lucht
Associate Editor